Available online at www.sciencedirect.com
ScienceDirect
Journal of Power Sources 161 (2006) 971–986
JOURNAL OF POWER SOURCES
www.elsevier.com/locate/jpowsour

Characterization and fault diagnosis of PAFC cathode by EIS technique and a novel mathematical model approach

Suman Roy Choudhury [a], Raghunathan Rengaswamy [b,*]

[a] *Naval Materials Research Laboratory, Ambernath Maharashtra, India*
[b] *Department of Chemical Engineering, Clarkson University, Potsdam, New York 13699, USA*

Received 6 February 2006; received in revised form 8 May 2006; accepted 9 May 2006
Available online 3 July 2006

Abstract

Considerable ongoing research exists in the area of fuel cells for power and distributed power generation. Of the various types of fuel cells, phosphoric acid fuel cell (PAFC) is a mature technology and is under limited production in various parts of the world. Electrochemical impedance spectroscopy (EIS) is a powerful tool which can be used for characterization of PAFC cathodes. In EIS, the electrode response is analyzed against an equivalent electrical circuit for diagnostics. A shortcoming of this approach is that multiple circuits can match the same response and correlating the physical electrode parameters with the circuit components may become quite difficult. To avoid this, a mathematical model of the PAFC cathode that is easy to solve is developed. The relative value and position of the maximum phase angle with respect to frequency is proposed as a diagnostic marker. A diagnostics table based on this marker is developed using the simulation of the mathematical model and the results are experimentally verified.

Keywords: PAFC; Dynamic model; Diagnostics; Spherical agglomerates; Electrode analysis

1. Introduction

The need for high efficiency, low emission energy conversion devices has attracted attention towards fuel cells the world over. A fuel cell is an electrochemical device which converts chemical energy to electrical energy directly. Out of the several families of fuel cells, hydrogen–oxygen fuel cells are the most important class of fuel cells for which the technology mature. Fuel cells have been used in the past in space applications. Other possible applications include small to medium sized stationary power generation plants, vehicle propulsion and various type of power sources for military use. Of the hydrogen–oxygen fuel cell systems, the phosphoric acid fuel cell (PAFC) system has been commercialized successfully. PAFC systems operate at 150–190 °C and pressure ranging from ambient to 5 atm. PAFC systems primarily use Pt as a catalyst both for hydrogen and oxygen electrodes. Operating temperature range of PAFC allows it to process hydrogen directly from hydrogen sources such as reformer gases. CO (less than 1%) present in the reformer gases are not adsorbed on Pt sites owing to high operating temperature. The other components used in a PAFC are mainly made of graphite and carbon. All of these make PAFC a versatile member of the hydrogen–oxygen fuel cell family.

PAFC systems, after evaluation by various groups (many of them are military groups such as the US marines) have reported excellent onsite power generation features. There are various features of the PAFC system that make it attractive. One example is the ability to have co-generation facilities using waste heat from the stack. Further, part of the waste heat can be used for process steam generation and can be fed to the upstream reformer. All these features allow overall system efficiencies to be about 80% [1]. High operating temperature (150 °C) results in high CO tolerance. This helps in the direct usage of reformer gas without CO filtration resulting in a reduction in the system complexity. However, there are some issues that need to be addressed for deeper penetration of PAFC systems. At present, for example, United Technologies Corporation (UTC) a market leader in PAFC systems is selling around 30–40 power plants per year but it is still around three times costlier for effective market penetration.

* Corresponding author. Tel.: +1 315 268 4423; fax: +1 315 268 6654.
E-mail address: raghu@clarkson.edu (R. Rengaswamy).

0378-7753/$ – see front matter © 2006 Published by Elsevier B.V.
doi:10.1016/j.jpowsour.2006.05.005

Nomenclature

a_a	effective area of catalyst site per unit volume of agglomerate ($cm^2\ cm^{-3}$)
b	normal Tafel slope (volts per decade)
c_{os}	concentration of oxygen on surface of agglomerate ($gmol\ cm^{-3}$)
C'_{cap}	capacitance per unit volume of agglomerate ($F\ cm^{-3}$)
c_{1a}	concentration of oxygen inside agglomerate ($gmol\ cm^{-3}$)
D_{agg}	diffusivity inside agglomerate for oxygen ($cm^2\ s^{-1}$)
D'_{agg}	diffusivity inside liquid encapsulation on agglomerate for oxygen ($cm^2\ s^{-1}$)
f	frequency of the induced sinusoidal potential (Hz)
F	Faraday constant (96,500 Coulombs per g equivalent weight)
H	Henry's constant for oxygen solubility in phosphoric acid ($gmol\ cm^{-3}\ Pa^{-1}$)
i_a	local current density ($A\ cm^{-2}$)
I_{agglo}	total current generated in the agglomerate (A)
i_0	exchange current density for oxygen reduction on Pt ($A\ cm^{-2}$)
k	reaction constant of oxygen reduction reaction
n	number of electrons taking part in the reaction
O_{rr}	oxygen reduction rate ($gmol\ s^{-1}\ cm^{-3}$)
p_1	partial pressure of oxygen (Pa)
r	radial dimension inside an agglomerate originating at the center (cm)
R_{agg}	average radius of an agglomerate (cm)
t	time (s)
T	system temperature in kelvin scale

Greek symbols

α	activation coefficient
ϵ	capacitance per unit area of the active catalytic sites ($F\ cm^{-2}$)
η	local overpotential (V)
η_{dc}	steady dc polarization (V)
κ_e	electrolyte conductivity ($\Omega^{-1}\ cm^{-1}$)
κ'_e	electrolyte conductivity inside agglomerate core ($\Omega^{-1}\ cm^{-1}$)
λ_r	porosity of the agglomerate

Cost reduction, efficiency and operational lifetime enhancement are the primary ways to reduce the effective cost of PAFC systems. Although the PAFC manufacturers claim around 40,000–50,000 h of life, the mean time before failure (MTBF) should be sufficiently high as well. This will make the system more reliable and acceptable for extensive use. Using cells that require thinner plates is a way to reduce cost. Further, this may make addressing local cell overheating problems simpler. However, the number of cells in a stack will increase. Usage of improved groove pattern for optimum flow distribution in the cell is another way to enhance the power density. All these modifications require extensive simulations with comprehensive distributed models capturing the features related to fluid flow, reaction kinetics, mass and heat transfer.

For successful long lifetime operation with high MTBF one has to address various issues related to the operation of the fuel cells. A short list of these are: gas cross over due to edge seal corrosion, acid loss, electrode starvation due to blockage, acid concentration change due to fluctuating load and unbalanced moisture control, fouling of electrode due to inlet impurities, and ambient moisture changes. All of these factors affect PAFC cathode performance by varying the wetting of the electrode. Changes in oxidation and reduction of groups on carbon catalyst support can cause acid flooding. Changes in oxidation and reduction can result from any of the following: carbon corrosion, expansion or contraction of acid volume. These can in turn be caused by the changes in concentration, reactant flows and the power demand. Thus the overall performance of the stack will depend upon the age as well on the operational history of the stack. In view of this, a diagnostic methodology that can identify the root cause of performance degradation is an important component in improving the operational lifetime of the installed PAFC systems.

Failure analysis is valuable from both off-line and on-line perspectives. Some of the commonly found failure analysis approaches for fuel cell systems are:

- Step tests of current or potential. This includes current interrupt methods for internal resistance measurement and analysis of settling time [2]. This is a simple technique but for an actual stack, high current handling electronics with high frequency data acquisition system is needed as the entire stack current will flow through the testing equipment. Further, such a transient method does not identify many of the common faults. For example, one can identify the change of internal resistance but it may not be possible to detect the root cause for such a change. For practical stacks, the test has to be done on the whole stack and it may not be possible to detect the faulty cells and the reason for the fault.
- Analysis by perturbing the flow and pressure monitoring can provide information about major blockages and associated problems. However, it might not be possible to detect typical electrode related phenomena such as the electrode flooding.
- Cyclic voltametry is suitable for off-line analysis to understand the changes in the catalyst electrochemical area.
- Electrochemical impedance spectroscopy (EIS) is a frequency response analysis technique that is performed by inducing a sinusoidal voltage or current over a steady state dc polarization. The resulting ac impedance related response of the electrode is analyzed. These tests are carried out either at a fixed amplitude (current/voltage) and various frequencies or at a fixed frequency by varying the potential/current. EIS is potentially a powerful tool that can provide rich information for the purpose of fault diagnosis. However, the results need to be analyzed through models. As only the ac perturbation needs to pass through the detector system, single cell/electrode (with appropriate probes) of a stack can be analyzed online. Fur-

ther, the sinusoidal amplitude is kept around 20 mV and it is possible to handle the total current generated by a stack for EIS studies.

1.1. Model selection

A porous electrode is a complicated structure, which is difficult to characterize at very small length scales. Various techniques have been attempted in the literature to characterize the porous gas diffusion electrodes. A cylindrical pore model [3] has been extensively studied to explain the three phase boundary (as discussed by Celikar et al. [4]). A thin film model was developed by Will [5] that includes the diffusion and polarization effects. An improvement to the thin film model was the double-scale-porosity theory [6]. However, this model suffers from assumptions related to linear diffusion.

Giner and Hunter [7] proposed a flooded agglomerate model as an improvement over the double-scale-porosity model. Their model considers that catalyst particles form porous electronically conductive cylindrical agglomerates filled with electrolyte, which extend through the thickness of the electrode. The surrounding hydrophobic channels are filled with reactant gas and the diffusion takes place in the radial direction. Iczkowski and Cutlip [8] proposed a spherical agglomerate model for characterizing the porous reaction layer.

Yamashita and Taniguchi [9] presented a slab like agglomerate partially filled with electrolyte. This work considers diffusion only in the direction orthogonal to the ionic flux. Perry et al. [10] and Celikar et al. [4] consider a spherical flooded agglomerate based reaction layer similar to the model developed by Iczkowski and Cutlip [8]. The array of spherical agglomerates form the catalyst layer in three dimensions and the intermediate space is filled with the diffusing gas. This type of modelling with a thin electrolyte coating on each electrolyte flooded (filled) agglomerate for ionic continuum has distinct advantages. The visualization of the reaction layer as an array of such spherical agglomerates – whose diameter is much smaller than the catalyst layer thickness – provides a good account of the physical processes involved. Fig. 1 depicts a scanning electron micrograph (SEM) of the PAFC cathode catalyst layer developed at NMRL. It can be clearly observed that the flooded spherical agglomerate characterization (Fig. 2) conforms well with the experimental characterization.

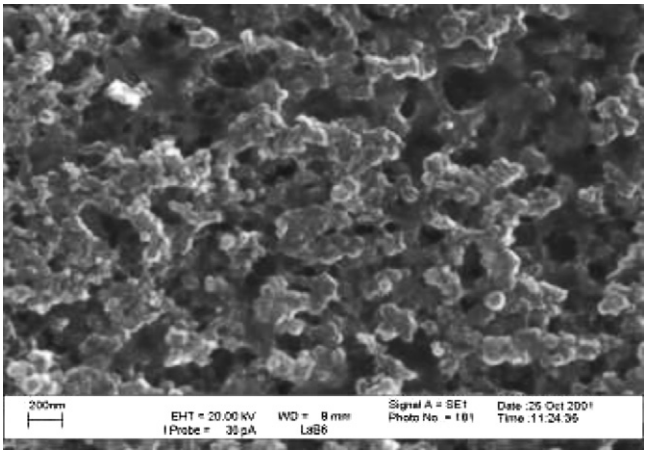

Fig. 1. SEM photograph of PAFC cathode catalyst layer.

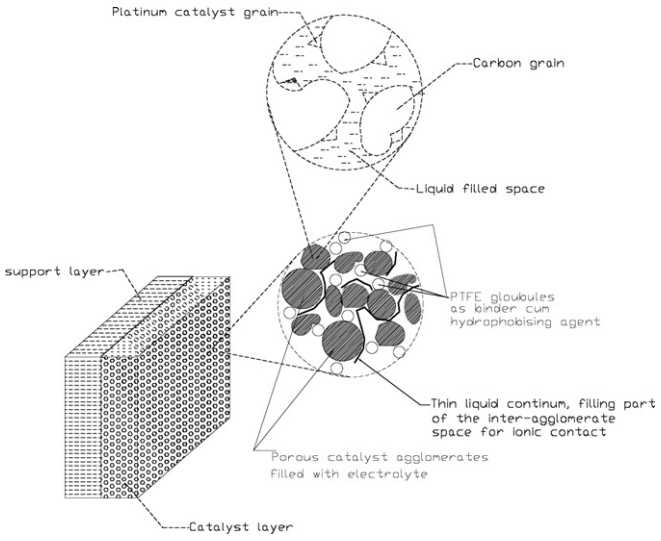

Fig. 2. Flooded electrolyte model.

1.1.1. Fault diagnosis and the proposed approach

Various practical aspects need to be addressed for successful development of a fault diagnosis system for fuel cells. PAFC cathodes change with time due to normal aging and the fault diagnosis system should be able detect the problem in the presence of normal ageing. Some of the approaches that model and fit the parameters too tightly may not possess the necessary flexibility to handle the normal changes that occur over time.

Fault diagnosis requires the identification of a distinct signature for every one of the faults. This can be achieved if a fault could be generated and the signature identification and subsequent matching is done experimentally. Another approach is to build a model for the system and introduce faults in the model for the development of diagnostic signatures and validate the diagnostic signature experimentally. From the fuel cell perspective, for easy experimentation, in the case of generic faults, the efficiency of the identified diagnostic signatures can be validated in small sized electrodes. EIS is a fault diagnosis tool that we believe can be used to identify a wide range of faults. However, fault analysis of the EIS results through the standard transmission line models might not be sufficient. This is because transmission line models could potentially generate multiple parameter values for the same data and multiple circuits are also possible. Correlating the parameter values in the form of resistances and capacitances to the physical fuel cell electrode parameters may prove to be difficult. Further, the total impedance based models are not very successful for comparing dissimilar electrode geometries.

In this work, a simple single spherical agglomerate physics based model is used for analysis. The utility and also the limitations of the proposed simple model in guiding the development

of diagnostics markers for use in complete electrode diagnosis will be discussed in the subsequent sections of this paper. It is important to make some observations about the proposed approach at this point. First, the impedance of a single representative spherical agglomerate cannot be quantitatively matched with that of the electrode, and this is not the intention in this paper. The basic motivation is to compare electrodes with different geometries from fault analysis viewpoint. The simple model is used only in guiding the development of the diagnostic marker, which will subsequently be validated on electrode data. Based on the predictions of the simple model, we will demonstrate that the position of the peak phase angle in the low frequency spectra can be used as a potential fault diagnostic marker. The peak phase angle position in the spectrum and its relative shift with respect to a normal electrode is easy to compare, qualitatively. It may be noted that the comparison of the magnitude of the peak phase angle can also yield valuable data but for that a complete electrode model needs to be solved. This will bring into question the complexity of the model development, parameter estimation and the final utility of such a model for fault diagnosis purposes. We do not attempt to answer these questions in this paper.

2. Unsteady state model of PAFC cathode for EIS analysis

This work is primarily focussed on failure analysis of phosphoric acid fuel cell (PAFC) cathode. For phosphoric acid fuel cell (PAFC) cathode, any problem such as electrode flooding, catalyst poisoning, blockage in the gas flow field, acid drying and gas cross over will have similar effect and the cell potential will drop. The steady state performance – while polarizing the cell at various current densities – does not usually reveal the type of problem that has occurred inside the cell. One way to ascertain the reason for failure is to excite the cell from the steady state and analyze the transient response. Variations in dynamic response for the different failure mechanisms allow dynamic electrochemical techniques to be used as a potential tool for diagnostics. For example, non-performance due to gas blockage under a sudden change in load will respond sluggishly, and for a short duration of time may even show near normal dynamic response. However, catalyst poisoning, will have a much faster response.

Various electrochemical methods are available for testing the dynamic response of an electrode, for e.g., cyclic voltametry (CV) also known as triangular pulse voltametry, electrochemical impedance spectroscopy (EIS) and so on. The use of these techniques for characterizing fuel cell electrodes has been reported by several researchers [11]. Among these, EIS is a very powerful tool which can be used to test and diagnose possible faults in PAFC electrode. One major advantage of this technique is that a non-invasive real-time analysis can be performed on a live stack. EIS is basically a small perturbation frequency response analysis. The cell is excited with a sinusoidal cell potential/cell current input on top of a steady dc load.

Electrochemical systems like fuel cells are highly non-linear in nature. However the EIS analysis is developed based on a linear system representation. Hence, the ac sinusoidal potential component has a very low amplitude, typically less than 20 mV. In this work, EIS analysis is done by inducing potential and measuring the current response. EIS results which are in the form of Nyquist and Bode plots, with impedance or admittance as the parameters, need to be analyzed. Generally, this is done by matching the EIS data with an equivalent electrical circuit comprising of elements such as resistors, capacitors, inductors, and warburg capacitor. Each of these circuit components is then related to the some of the physical characteristics of the electrode like diffusion resistance, catalyst activity, etc. [12]. A major problem with this approach is that multiple circuits can be used to match the same response characteristics which often yields misleading results. To circumvent this problem, in this work, the EIS data is proposed to be analyzed using a dynamic distributed parameter model of a PAFC cathode for diagnostics. The advantage of this method is that direct analysis of physical parameters such as active catalyst area, diffusion resistance and so on is possible. The position and relative value of the phase angle with respect to frequency is used as a diagnostic marker for PAFC cathode diagnostics. A diagnostic table using this marker is developed by solving a simple mathematical model and the results are validated experimentally. The experimental studies have been carried out on PAFC electrodes developed at Naval Materials Research Laboratory (NMRL), DRDO, India.

2.1. Reaction layer

In this section, we will focus on the model used for characterizing the reactions occurring in the electrode. Modelling of the reaction layer can be done by using the flooded agglomerate structure [10,4] coupled with gas diffusion equations. A steady state two-dimensional model using the flooded agglomerate model has already been discussed in our previous work [13]. An agglomerate is a mixture of carbon, the electrolyte (fully flooded) and platinum. Each agglomerate is considered to be completely coated with electrolyte, through which the reactant diffuses. This layer is responsible for maintaining an electrolyte continuum all through the electrode. To model this characterization, an agglomerate is considered to be composed of two concentric shells. In the outer thin shell only liquid diffusion of oxygen takes place. Inside the inner core reaction as well as diffusion occurs. The outer layer is expressed as a fraction of the overall diameter of the agglomerate. For a very thin outer film, the steady state dc current may not be affected much, but this layer can change the transient response to a great extent.

Oxygen transport inside the agglomerate undergoing reaction can be written as:

In the outside liquid diffusion shell:

$$(D'_{\mathrm{agg}}/r^2)\partial/\partial r(r^2\partial c_{1\mathrm{a}}/\partial r) = \partial c_{1\mathrm{a}}/\partial t \tag{1}$$

In the inside active core:

$$(D_{\mathrm{agg}}/r^2)\partial/\partial r(r^2\partial c_{1\mathrm{a}}/\partial r) = -O_{\mathrm{rr}} + \lambda_{\mathrm{r}}\partial c_{1\mathrm{a}}/\partial t \tag{2}$$

where λ_{r} is the porosity inside the agglomerate. For simulation purposes, it is considered to be equal to the overall reaction layer

porosity:

$$-O_{rr} = (a_a i_a/nF) = (a_a i_o/nF)(c_{1a}/c_{os}) \exp(-2.3\eta/b)$$
$$= a_a k c_{1a} \exp(-2.3\eta/b) \quad (3)$$

where $k = i_o/(nFc_{os})$.

The reverse reaction, i.e., oxygen evolution reaction term is neglected in Eq. (3), as the contribution of the reverse reaction will be significant only for near open circuit condition, i.e. +75 mV from the equilibrium value [14]. Tafel slope calculation is performed considering "α (activation coefficient)" to be 1/2 over platinum.

2.2. Calculation of overpotential distribution

Overpotential distribution can be determined by using ohms law for proton movement inside the agglomerates and considering no accumulation of protons inside the agglomerates other than in the double layer near the active sites.

At the liquid diffusion part of the agglomerate:

$$\kappa_e/(Fr^2)\partial/\partial r(r^2 \partial\eta/\partial r) = 0 \quad (4)$$

In the inside active layer:

$$\kappa'_e/(Fr^2)\partial/\partial r(r^2 \partial\eta/\partial r) = n(-O_{rr} + C'_{cap}/(nF)\partial\eta/\partial t) \quad (5)$$

where

$$C'_{cap} = a_a \epsilon \quad (6)$$

2.3. Boundary conditions of the agglomerate

$$r = R_{agg}, \qquad c_{1a} = c_{os}, \qquad \eta = \eta(t) \quad \forall t \quad (7)$$

$$r = 0, \qquad (\partial c_{1a}/\partial r) = 0, \qquad (\partial\eta/\partial r) = 0 \quad \forall t \quad (8)$$

and

$$c_{os} = Hp_1 \quad (9)$$

This equilibrium relationship assumes Henry's law for the oxygen solubility in acid [13], where oxygen partial pressure (p_1) at the liquid encapsulated agglomerate surface is known. A flux balance at the interphase of agglomerate and liquid encapsulation is written:

$$D'_{agg}(\partial c_{1a}/\partial r) = D_{agg}(\partial c_{1a}/\partial r), \qquad \kappa_e(\partial\eta/\partial r) = \kappa'_e(\partial\eta/\partial r),$$
$$r = r_{interphase} \quad \forall t \quad (10)$$

where D'_{agg} is the diffusivity of oxygen in the liquid shell.

Initial condition at time = 0 is based on the system start up. One such condition is the open circuit condition for which:

$$c_{1a} = c_{os}, \qquad t = 0 \quad \forall r \quad (11)$$

For determining instantaneous current generated inside an agglomerate local reaction rate added with reaction due to capacitance effect is integrated over the entire agglomerate volume and expressed in current equivalent. This is as follows:

$$I_{agglo} = nF \int_0^{R_{agg}} 4\pi r^2 \{O_{rr} + C'_{cap}(\partial\eta/\partial t)\}\, dr \quad (12)$$

3. Proposed approach

The dynamic agglomerate model discussed in the previous section can be integrated with our previous work [2] and can be solved to analyze the sinusoidal frequency response. However, such detailed distributed model will require high computational power along with longer solving time. In this work, a study of the agglomerate model for PAFC systems is undertaken to demonstrate the feasibility of developing diagnostic markers for cathode diagnostics. The effect of the various electrode parameters on a newly proposed diagnostic marker is studied. The generalization of this approach for a complete cathode analysis is demonstrated through detailed experimental results. In the proposed approach, variation of the output, i.e., the phase lag of the total current when excited with a sinusoidal potential input while the system is polarized with a steady overpotential is analyzed for various parameters. Distinct signatures that can be used as diagnostic markers are derived based on this analysis. This then forms the basis for cathode diagnostics. The proposed approach also allows geometrically dissimilar electrodes to be analyzed. We will demonstrate that, for example, the output from a small unit cell PAFC data can be tuned with the model output and the results can then be used to understand a problematic cell in a big stack. For this analysis, $\eta(t)$ in Eq. (7) is:

$$\eta(t) = \eta_{dc} + A \sin(2\pi ft) \quad (13)$$

For example, if a 100 mV steady polarization with a 10 mV amplitude sinusoidal excitation of frequency f is induced then

$$\eta(t) = -0.1 + 0.01 \sin(2\pi ft) \quad (14)$$

3.1. Adjustment of electrolyte resistance for single agglomerate analysis

In order to validate the simulated response of the agglomerate model, the solution (electrolyte) resistance of the thin electrolyte shell covering the agglomerate needs to be adjusted. Otherwise, the value of the phase angle as well as the position of the peak phase angle may not be proper as the experimental and simulated values of the ratio of overall resistance to capacitance should be similar. Thus the resistance of the electrolyte shell is adjusted, as the experimental results will consider the entire resistance of the electrolyte from the electrolyte–electrode interface. This effect is illustrated in Fig. 3. The desired effect can be achieved by decreasing the specific conductance of the electrolyte film covering the agglomerate so that the total conductance is of the same order as the overall ion path resistance as shown in Fig. 3.

Unless mentioned otherwise all the parameters that are used are mentioned in Table 1. The unsteady state agglomerate model is solved using PDEASE-2D package [13,2]. The time dependent part is solved using a marching forward method.

4. Model analysis

In this section, a study of the agglomerate model is undertaken to validate the basic idea proposed in this paper. Parameters such as electrolyte resistance, agglomerate size, capacitance per unit

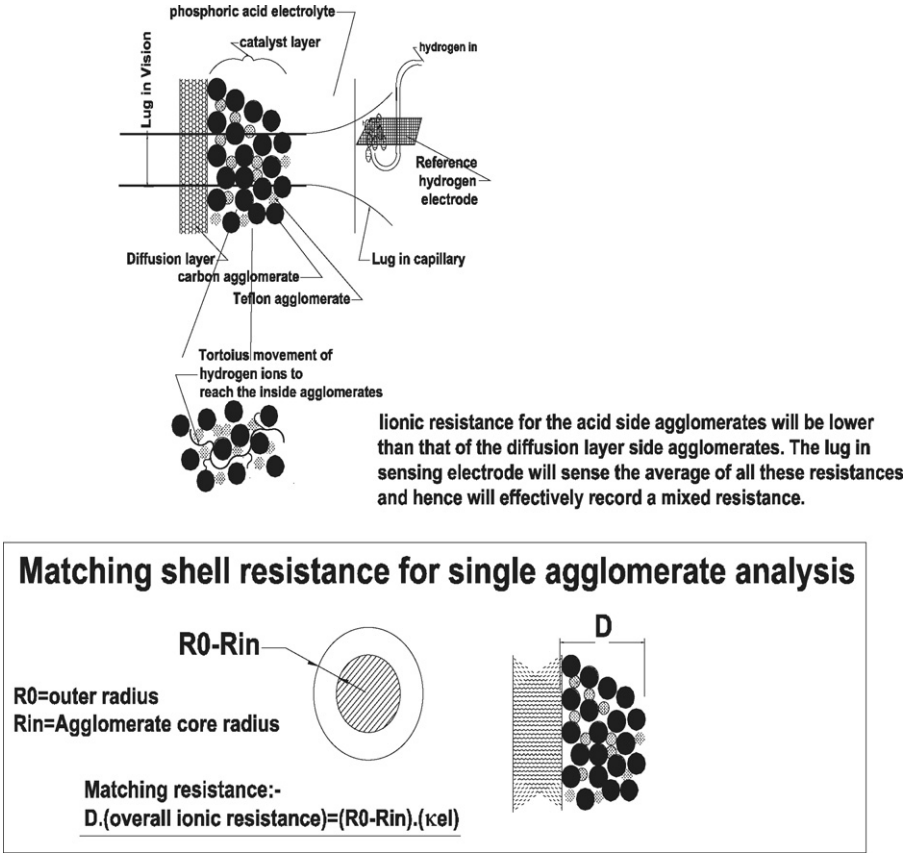

Fig. 3. Electrolyte resistance adjustment for agglomerate analysis.

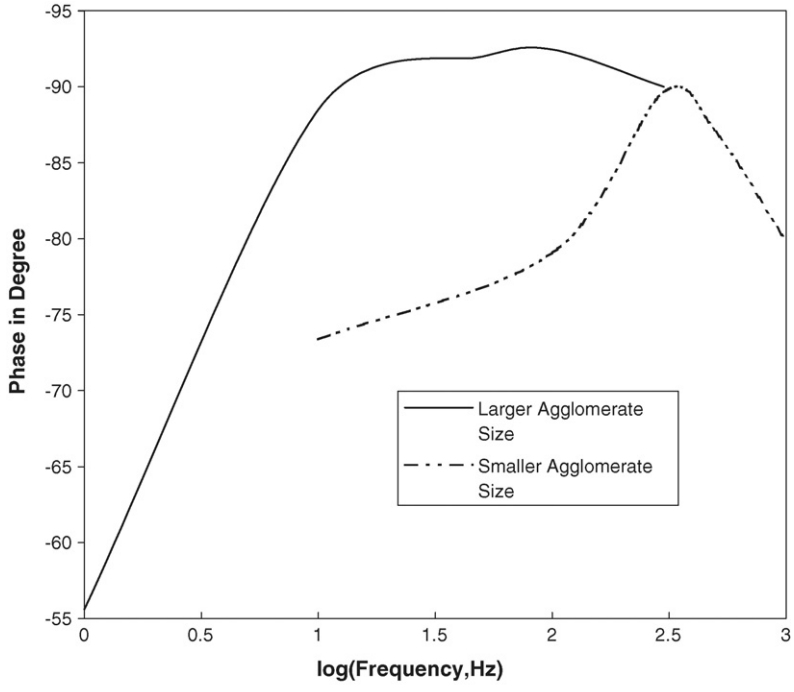

ε	R_{agg}	a_a	κ_{el}	κ_{agg}	η
20e-06	5e-03& 5e-04	35000	1e-06	0.4	-0.1

Fig. 4. Simulated phase angle plot for different agglomerate sizes.

Table 1
Values of parameters

Parameter name	Value	Remark
a_a	3.5e−04 ($cm^2\ cm^{-3}$) of agglomerate	Experimental
b	120 mV per decade	Tuning
D_{agg}	1.0e−04 ($cm^2\ s^{-1}$)	Literature
H	5.5e−13 ($gmol\ cm^{-3}\ Pa^{-1}$)	Literature
i_0	1.0e−06 ($A\ cm^2$)	Literature
n	4	Stoichiometry
R_{agg}	1.0e−04 (cm)	SEM picture
Reaction layer	400 μm thick	Experimental
T	(150 + 273) K	Experimental
κ_e	0.5 ($\Omega^{-1}\ cm^{-1}$)	Literature [13]
λ_d	0.5	Experimental
λ_r	0.5	Experimental
D'_{agg}	D_{agg}/λ_r	Literature
κ'_e	0.25 ($\Omega^{-1}\ cm^{-1}$)	Literature
p_1	10^{05} (Pa)	
Shell fractional thickness	0.9 of the total agglomerate radius	

active area (ϵ) are varied and their impact on the phase lag is studied. In Section 5 these results will be validated experimentally.

In Fig. 4 the simulated phase angle plot is shown for two different agglomerate sizes at an overpotential of 100 mV. It can be seen that the bigger agglomerate peak phase angle occurs at a lesser frequency than the smaller agglomerate. If the dissolved oxygen concentration and its gradient are significant inside the agglomerate, then the effect of diffusion will contribute more towards the phase angle in form of pseudocapacitance which acts in series with the reaction current. Thus, the phase angle peak at lesser frequency indicates more reaction inside the agglomerate core than at the surface. The higher frequency is not able to interact with the deep seated reaction sites. The peak shape of the larger agglomerate size is quite broadened out as well. As for the smaller agglomerate size, the diffusion area and the depth of the core is somewhat smaller. This allows the higher frequency to interact with the pseudocapacitance, and thus the peak phase angle for smaller size is shifted towards the higher frequency side.

The effect of change of active area is depicted in Fig. 5. It can be seen that for higher active area (a_a), the peak phase angle appears at a relatively lower frequency than lower active area. This is somewhat against the expectation because for lower active area density, the chance of reaction contribution from the core is enhanced. Thus the peak phase angle must be at a lower frequency for the less active area. This simulation result can be explained as below. It is considered in the model that the double layer capacitance is based on the active area density. For lesser a_a, the total double layer capacitance is also less, and in this case, is dominant over the diffusion related pseudocapacitance effect. Unlike the pseudocapacitance effect of diffusion, the double layer capacitance acts in parallel to the main reaction current. This allows the peak phase angle to shift towards the higher frequency side for a lesser a_a. A parametric analysis is

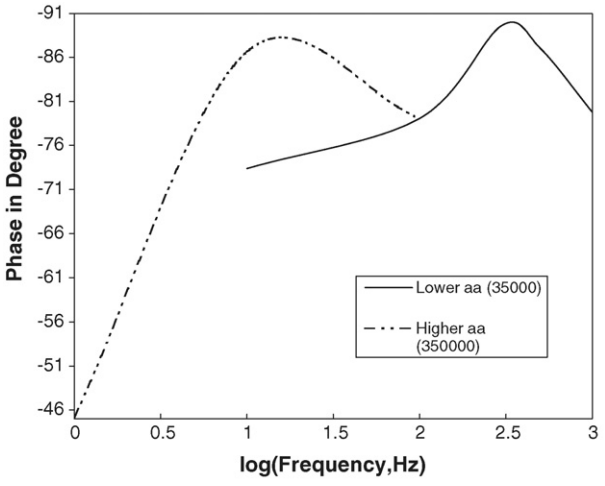

ε	R_{agg}	a_a	κ_{el}	κ_{agg}	η
20e-06	5e-04	35,000& 3,50,000	1e-06	0.4	-0.1

Fig. 5. Simulated phase angle plot for different active areas.

performed to test the theory discussed above. In this case the effect of variation of active area density (a_a) is considered but the capacitance value (ϵ) of the lower a_a is so adjusted that the total capacitance value remains the same. This can be physically considered as a case of active area fouling without hampering the double layer capacitance of the fouled active area.

The phase angle plot is depicted in Fig. 6. It can be seen that in the higher active area density (a_a) case, the peak phase angle is at the higher frequency side. This trend is exactly opposite to that discussed before. However, this otherwise fits into the explanation that higher a_a consumes most of the reactants at the surface and the core reaction contribution is less. Also, the main concentration gradient is at the surface and hence the ions can

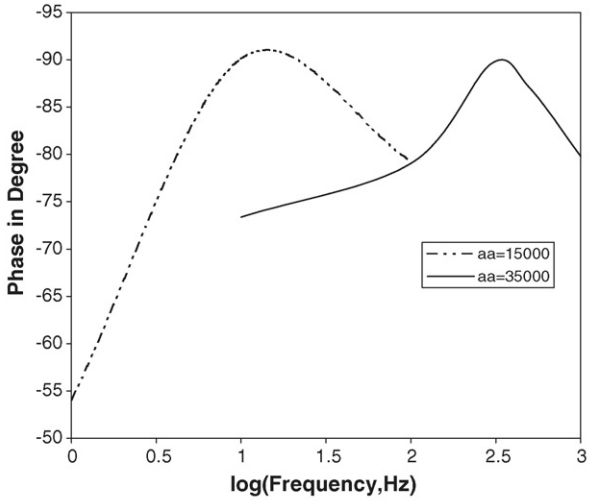

ε	R_{agg}	a_a	κ_{el}	κ_{agg}	η
20e-06	5e-04	35000	1e-06	0.4	-0.1
20e-06.(35000/15000)	5e-04	15000	1e-06	0.4	-0.1

Fig. 6. Simulated phase angle plot for different active areas but same total double layer capacitance.

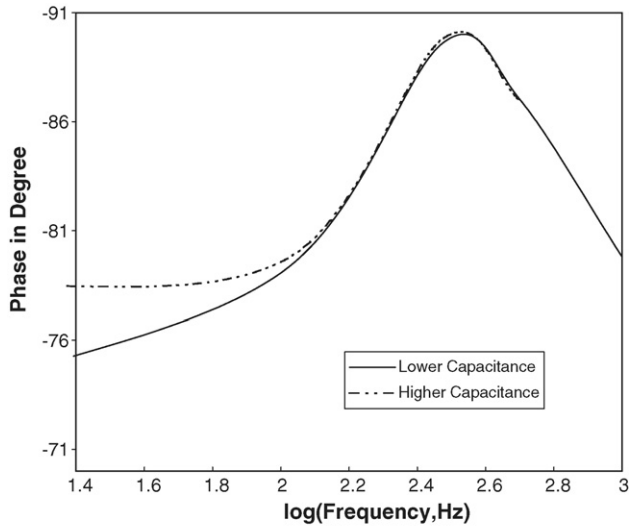

ε	R_{agg}	a_a	κ_{el}	κ_{agg}	η
20e-06& 10e-05	5e-04	35000	1e-06	0.4	-0.1

Fig. 7. Simulated phase angle plot for different double layer capacitances at lower overpotential.

interact at higher frequency. As the total double layer capacitance is forced to remain same, the reverse effect of the double layer capacitance is eliminated. The other parameter analyzed is the effect of double layer capacitance (ϵ). Fig. 7 depicts phase angle response of a different ϵ at an overpotential of 100 mV. It can be seen that the peak phase angle is almost located at the same place. Fig. 8 depicts the simulated performance of the same parameter at a higher overpotential of 200 mV. It can be seen that the peak phase angle for higher ϵ appears at a lesser frequency than the higher one. This effect can be analyzed if we consider that the double layer capacitance works in parallel to

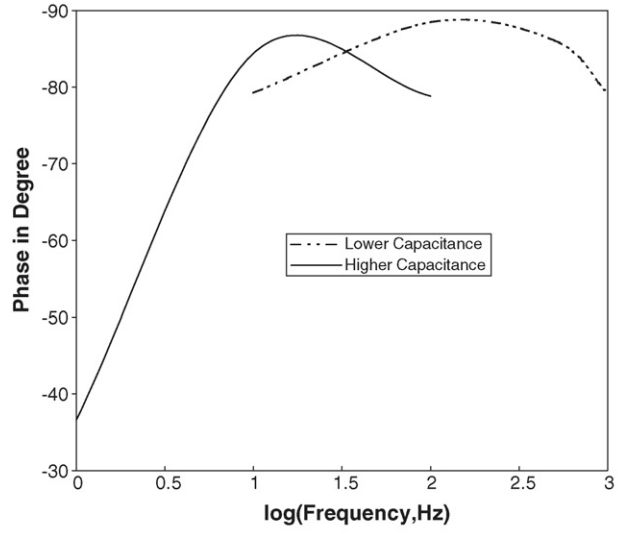

ε	R_{agg}	a_a	κ_{el}	κ_{agg}	η
20e-06 & 10e-05	5e-04	35000	1e-06	0.4	-0.2

Fig. 8. Simulated phase angle plot for different double layer capacitances at higher overpotential.

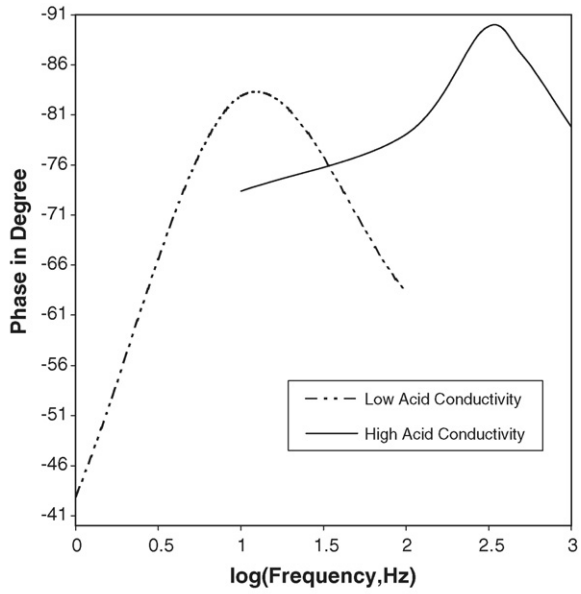

ε	R_{agg}	a_a	κ_{el}	κ_{agg}	η
20e-06	5e-04	35000	1e-06	4e-06 & 0.4	-0.1

Fig. 9. Simulated phase angle plot for different electrolyte resistances.

the reaction current. Thus a smaller capacitance requires higher frequency to achieve the peak phase angle. For smaller overpotential, the reaction current may not be high enough to separate the peak appreciably. Interestingly, this inability to separate the peak can be used as a effective tool in fault diagnosis purpose.

The effect of electrolyte (phosphoric acid) conductivity is shown in Fig. 9. The higher conductivity system shows peak phase angle at a higher frequency. This is as expected since the acid resistance acts in series to all the capacitance and the reaction current. This is due to hydrogen ion being the primary ion for all the current generation inside the electrolyte medium which is controlled by the electrolyte resistance. In Fig. 10, the same parameters are simulated, but at a higher overpotential of 200 mV. Here also the trend remains similar.

5. Experimental validation

In this section, experimental evidence is presented to verify the basic simulation results presented in the previous section. First, the experimental setup for EIS analysis is described followed by detailed experimental data to support the approach discussed in this paper.

5.1. Experimental setup for EIS analysis

Porous gas distribution electrodes (GDE) are made using Toray-120 porous conducting carbon paper and NMRL developed catalyst (Pt on carbon-Vulcan XC-72R) and Teflon suspension. At first, the carbon paper is wet proofed with the Teflon suspension and sintered. Further, the catalyst and Teflon suspension is mixed with iso-propanol to form a flock which is roll coated on the wet-proofed carbon paper. The catalyst used for this study is the second generation catalyst developed in NMRL

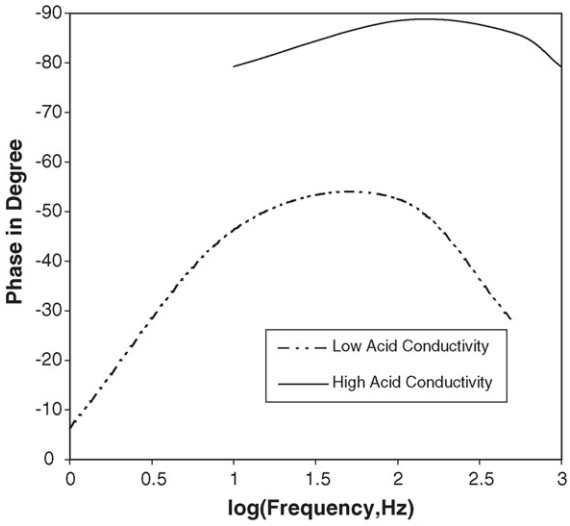

ε	R_{agg}	a_a	κ_{el}	κ_{agg}	η
20e-06	5e-04	35000	1e-06	4e-06& 0.4	-0.2

Fig. 10. Simulated phase angle plot for different electrolyte resistances at higher overpotential.

and its polarization performance is better than the catalyst used previously for validating the steady state model. The new catalyst developed in NMRL is in the lines of the method mentioned in the US patent [15]. The catalyst powder loading is 7 mg cm^{-2} of the paper. Typical standard of 10% Pt on carbon catalyst makes Pt loading at 0.7 mg cm^{-2} of the electrode. Teflon content is kept at around 40 wt.%. This Teflon percentage is found to be sufficient to prevent electrode flooding while keeping enough wet pores for reaction to occur.

The setup used is an unit cell setup as shown in Fig. 11. The setup consists of two planar graphite electrodes, viz., the cathode and anode, separated by a porous SiC matrix which holds the syrupy phosphoric acid electrolyte. The exposed area of the cathode is 20 cm^2. The cathode-matrix-anode is sandwiched between two grooved graphite plates which feed oxygen to the cathode and hydrogen to the anode. Two stainless steel plates act as the current collector at the two ends and all these are pressed by two end pusher plates which are electrically isolated. In order to test the effect of only cathode against a standard reference electrode, the matrix is connected to a standard hydrogen electrode (SHE) as a reference, through a glass filter paper (Merck GF120) wet with dilute phosphoric acid to make an ionic bridge. The "AutoLAb" potentiostat/galvanostat coupled with FRA is used to record the current response of the sinusoidal potential excitations on top of a steady dc load.

In order to check primary trend analysis for diagnostic purposes the electrodes are prepared as described here. All the cathodes are conditioned for several hours in 90–93% H_3PO_4 basis, by maintaining a cell potential of 0.7 V with respect to SHE in order to ensure complete wetting at a temperature of 150 °C. Several electrodes are prepared and readings are taken. An average of the readings are taken into consideration to avoid minor preparation errors. All the experiments are conducted with pure oxygen at 1.0 atm pressure at the cathode to compare the results with the model assumption.

5.2. Experimental results

The effectiveness of selecting the maximum phase angle position in the frequency spectrum as a diagnostic marker is tested experimentally. Some of the electrode properties are deliberately altered to see whether any change in the position of the maximum phase angle occurs in the phase angle plots.

5.2.1. Effect of active area

In order to study the effect of active area, two type of catalysts are used. The first one is a standard 10% Pt while the other is only 1% Pt loaded on Vulcan XC-72R carbon support. The catalyst loading on the electrode samples are 7 mg of Pt loaded carbon powder per cm^2 of the electrode for both the cases. Thus the active metal (Pt) is 0.7 mg cm^{-2} for the first case, whereas it is 0.07 mg cm^{-2} in the second case. The rest of the electrode manufacturing process, i.e., PTFE content, sintering cycle, etc.

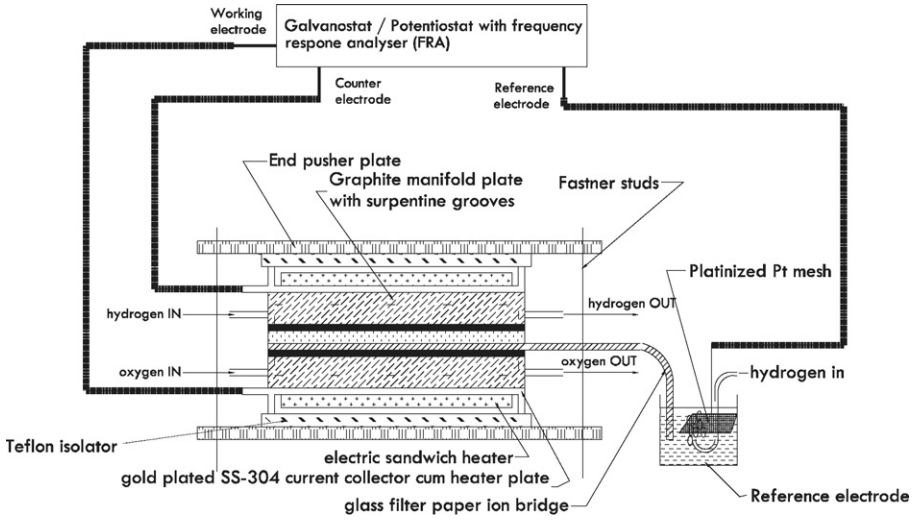

Fig. 11. Unit cell experimentation setup for impedance spectroscopy.

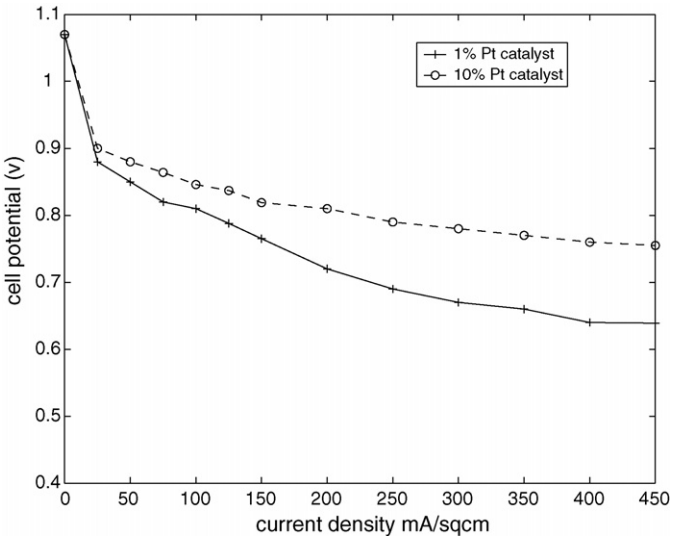

Fig. 12. dc polarization unit cell result of 1% Pt loaded catalyst against standard one.

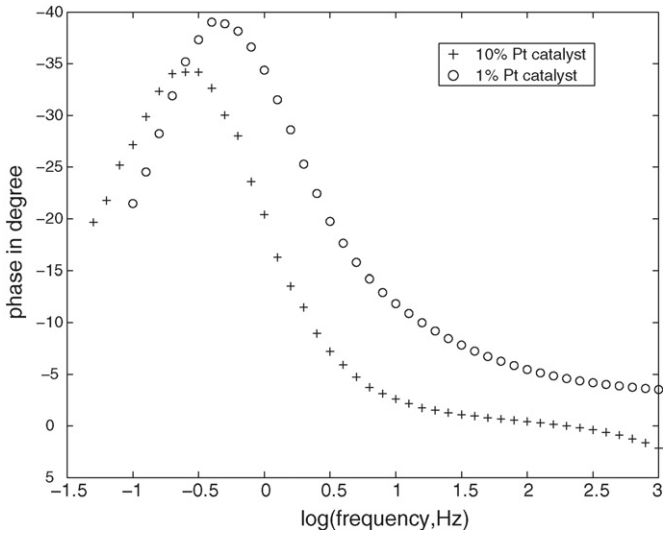

Fig. 14. Experimental phase angle plot for different Pt loading at $\eta = -0.1$ V.

are same for both the electrodes. The catalysts used are proprietary of NMRL and shows lower electrochemical area for the 1% Pt than the 10% Pt catalyst. It is to be noted that although the Pt content of the second one is 1/10th of the standard one, the active area difference is less than that. This is due to the fact that the dispersion of Pt is better at lesser loadings and hence also the percent metal utilization.

Fig. 12 depicts the polarization performance of the 1% Pt catalyst along with the standard 10% Pt. The performance of the 1% Pt catalyst is found to be lower than the standard one as expected. Fig. 13 depicts the experimental Nyquist plot of the standard 10% Pt catalyst electrode along with 1% Pt. The high frequency impedance shows same electrolyte resistance. Fig. 14 depicts the experimental phase angle plot of the above mentioned electrodes. It can be seen that peak phase angle for the 1% Pt electrode is on the higher frequency side. Thus from the experimentation it can be seen that the position of the maximum phase angle has changed its position in the frequency spectrum

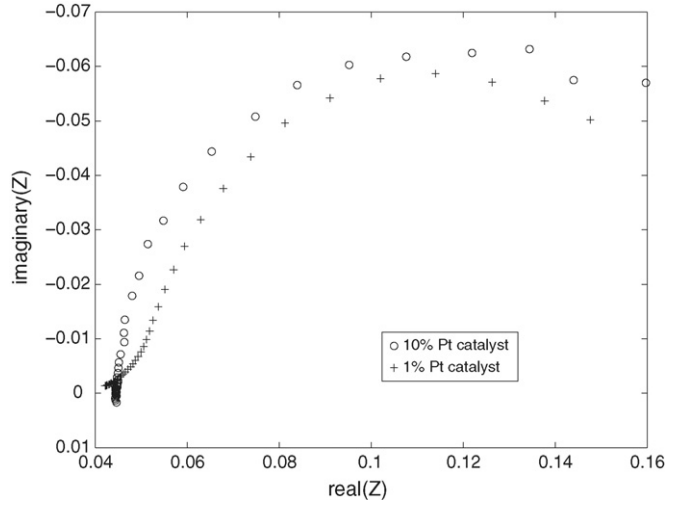

Fig. 13. Experimental Nyquist plot for different Pt loading at $\eta = -0.1$ V.

when the active area is changed. This change is more distinct than the electrode impedance plotted in the Nyquist plot as shown in Fig. 13.

5.2.2. *Effect of electrode fouling*

Further to the above mentioned effect of change of a_a, another experiment is designed to understand the response of a purposely fouled electrode. For actual stacks, the edge of the electrodes are required to be sealed with phenolic resins in a furfuryl alcohol base. Hence to check the effect of furfuryl alcohol contamination, the electrode sample is exposed to furfuryl alcohol vapor. Subsequently the sample is soaked in hot phosphoric acid as mentioned in the experimentation section before. The alcohol under high acidic medium is expected to be polymerized followed by partial charring. Presence of alcohol in the electrode after acid soaking is confirmed by testing the acid through infrared spectroscopy. Fig. 15 depicts the comparative spectroscopic data of the furfuryl alcohol and the concentrated acid after soaking. The data clearly shows that the acid contains alcohol traces.

This electrode is operated and conditioned in unit cell as mentioned in the experimentation section. Fig. 16 shows the dc polarization data of the alcohol initiated fouled electrode and a standard 10% Pt electrode. It can be seen that the performance of the fouled electrode is quite less particularly at higher current densities. Fig. 17 depicts the Nyquist plot of the two electrodes at an overpotential of 100 mV. It can be seen that the basic electrolyte resistance for both the cases are essentially same as the high frequency impedance at the left side bottom of the curve indicates. Hence the acid property is not affected by trace alcohol addition. The Nyquist plot also shows higher polarization for fouled electrode by the larger loop as expected than the standard good electrode.

Fig. 18 depicts the phase angle plot of the fouled electrodes along with a standard good cathode at an overpotential of 100 mV. It is seen that the peak phase angle of the fouled electrode has shifted to the left hand side. Further at a higher overpotential (at 200 mV), the same experiment is carried out.

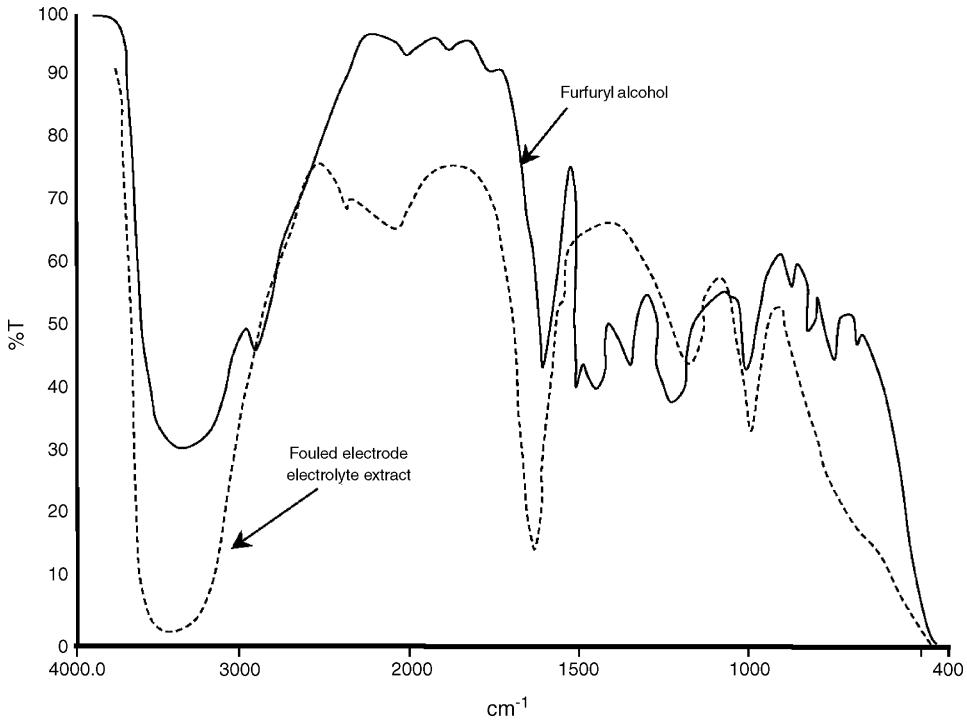

Fig. 15. Infra-red spectroscopy data of furfuryl alcohol and acid extract of fouled electrode.

Figs. 19 and 20 depict the Nyquist and phase angle plots, respectively of the electrode. The phase angle plot shows similar trend with the peak phase angle for the fouled electrode shifting to the left hand side. Thus it is observed that for a fouled electrode the trend remains similar at higher overpotentials also.

5.2.3. *Effect of electrolyte conductivity*

Change of acid concentration inside PAFC system causes change of the acid conductivity. The change of acid concentration occurs due to difference in humidification, change of flow rates or electrical loads, etc. An experiment is performed to observe the response of phase angle for change of acid concentration. The conductivity can be measured online easily by measuring the impedance at a reasonably high frequency. Such single point measurement often suffices for continuous steady state operation of PAFC stacks. However, this kind of measurement does not give all the necessary information if the stack is being operated under start–stop mode. A stack which is seeing frequent gas on for few hours followed by a shutdown, while maintaining the temperature of the stack, tends to lose acid faster in the cathode. This is due to the fact that under steady state operation a concentration gradient exists across the cell. The anode side gets diluted and the cathode side is concentrated. Thus the water flux is from anode to cathode side and water gets evaporated into excess oxygen stream.

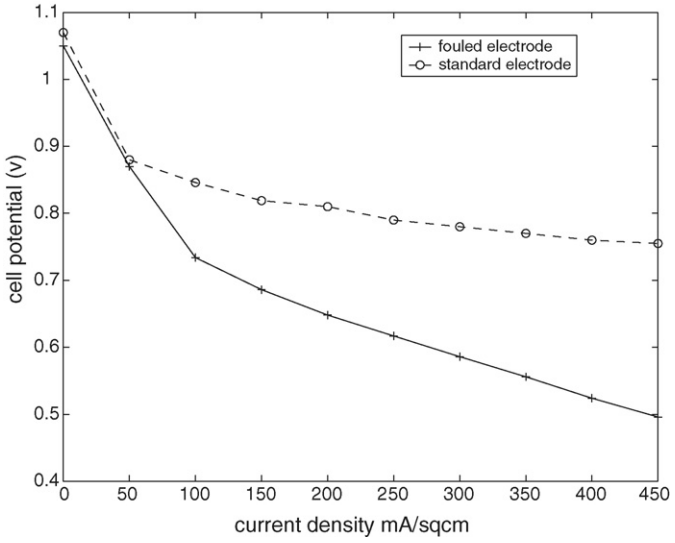

Fig. 16. dc polarization unit cell result of fouled electrode.

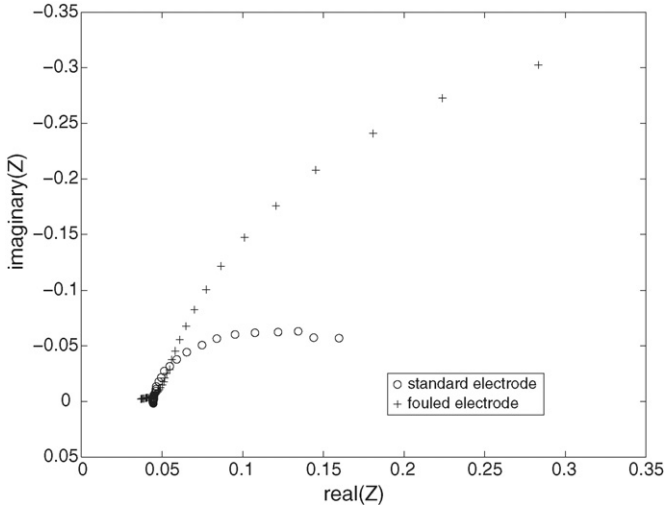

Fig. 17. Experimental Nyquist plot for fouled electrode at $\eta = -0.1$ V.

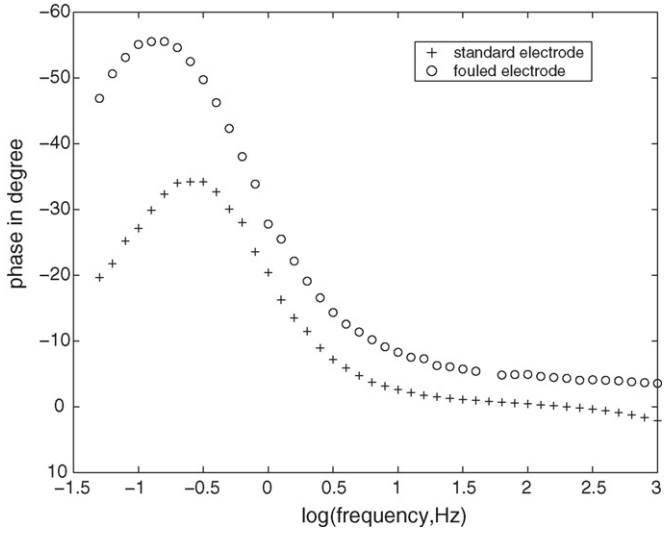

Fig. 18. Experimental phase angle plot for fouled electrode at $\eta = -0.1$ V.

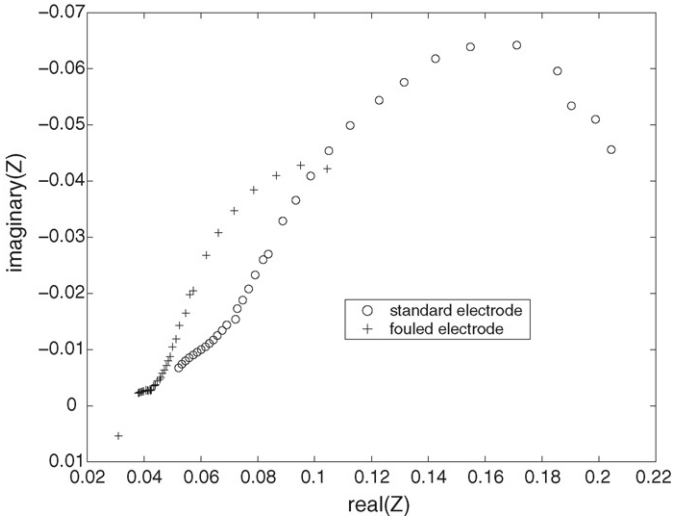

Fig. 19. Experimental Nyquist plot for fouled electrode at higher overpotential $\eta = -0.2$ V.

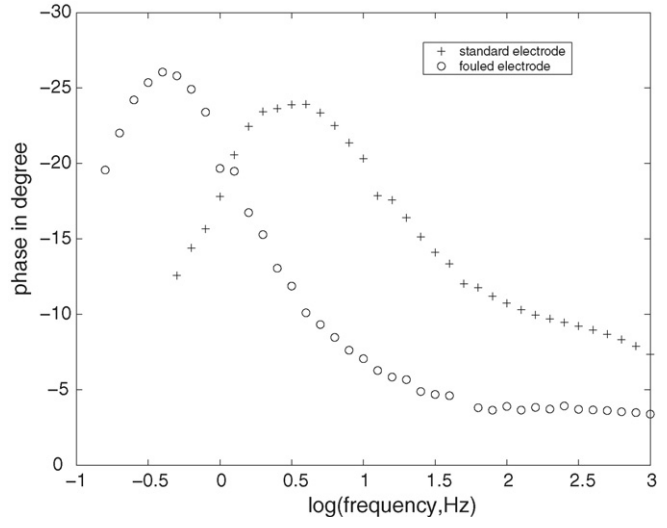

Fig. 20. Experimental phase angle plot for fouled electrode at higher overpotential $\eta = -0.2$ V.

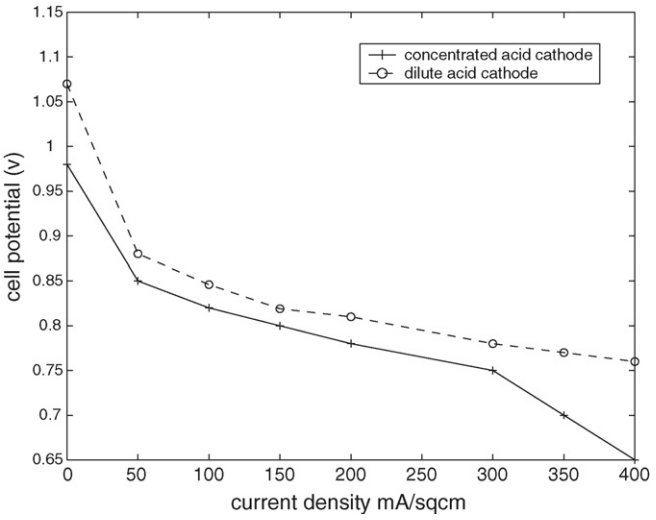

Fig. 21. dc experimental polarization result of concentrated acid cathode.

The effect of overall change of acid conductivity is created by taking a standard mature cathode and exposing the same to a higher concentrated acid and keeping the same in an oven overnight. After this, the electrode is mounted on the unit cell setup, and the cell is operated around a constant current density of 200 mA cm^{-2} for 1/2 an hour before the dc polarization and impedance spectroscopy is done. It is to be noted that at a given temperature, for concentrated phosphoric acid, the conductivity decreases with increase in concentration [16]. Fig. 21 depicts the comparative polarization of the concentrated acid sample against the standard electrode. It can be seen that the performance is reduced as expected for the concentrated acid sample. Fig. 22 shows the Nyquist plot of the sample electrode with respect to the standard one. It can be clearly seen that the acid conductivity of the concentrated acid sample is lower than the standard one from the high frequency impedance data which is the left side impedance data of the Nyquist plot. Fig. 23 shows the phase angle response. It can be seen that the concentrated acid sample having lower conductivity is shifted towards the left hand side.

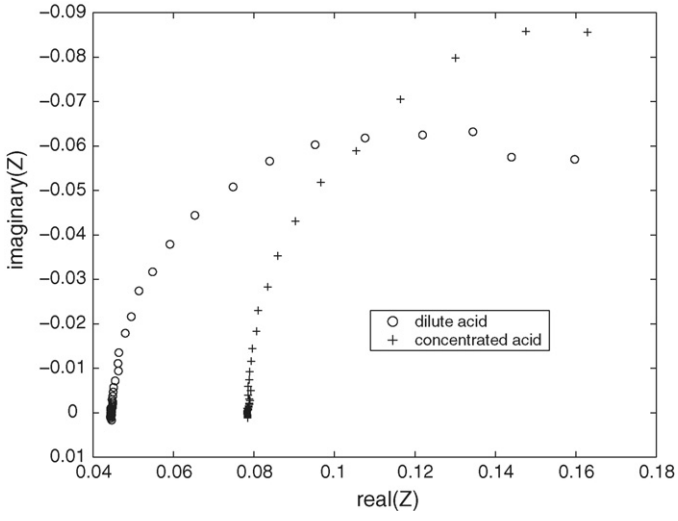

Fig. 22. Experimental Nyquist plot of concentrated acid cathode at $\eta = -0.1$ V.

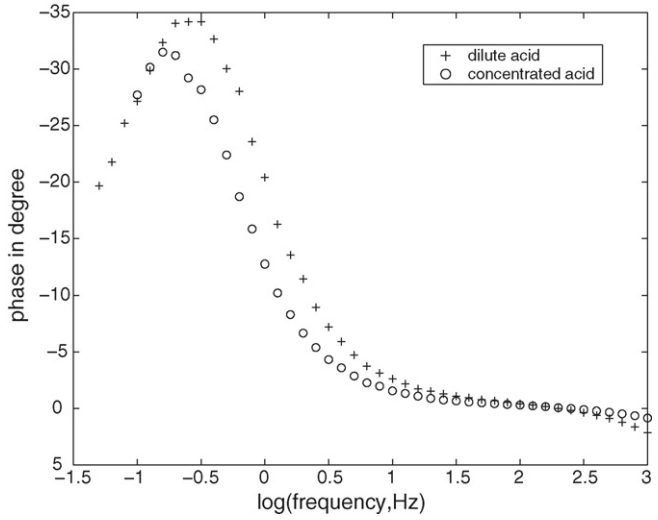

Fig. 23. Experimental phase angle plot of concentrated acid cathode at $\eta = -0.1$ V.

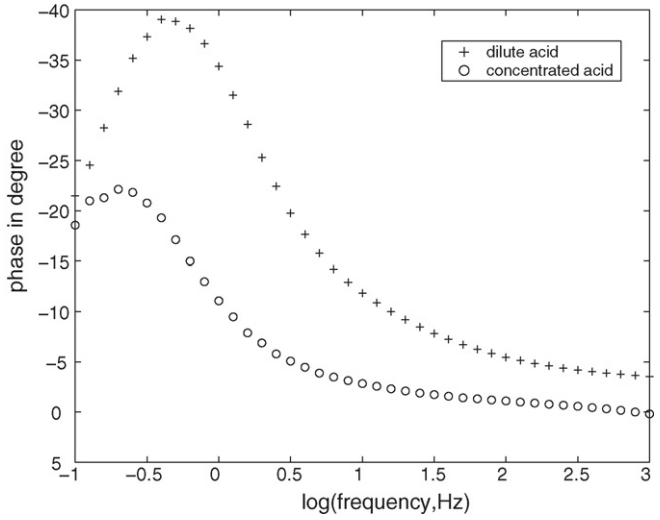

Fig. 25. Experimental phase angle plot of concentrated acid cathode at higher overpotential $\eta = -0.2$ V.

The same sample is similarly analyzed at a higher overpotential and the trend is similar to that shown in the Nyquist plot depicted in Fig. 24 and phase angle plot in Fig. 25.

6. Model analysis of experimental results

Experimental verification of the model output requires proper tuning of the model parameters so that realistic matching can be done. The major advantage of the proposed model is that the various physical parameters of the actual electrode system can be obtained experimentally and the values can be incorporated directly into the model. For other popular analysis techniques, which are based on transmission line LCR type models, one has to provide equivalent resistance, capacitance and so on based on indirect methods which may cause a number of problems ranging from inconclusive values to multiple choices yielding totally different results. In contrast, the mathematical model developed directly simulates the physical system and provides better understanding of the overall process. Another advantage of this system is that it allows manipulation of data to validate various hypotheses. However this should be done after considering the limitations of the model as described in the section later. A typical example of this aspect is discussed in the previous section where the overall capacitance is kept constant while varying the active area density. Out of the various types of parametric variation in the model, few can be verified experimentally. The others are so inter-related, that isolating them may be difficult. Some of the effects which can be studied experimentally are discussed in the following paragraphs.

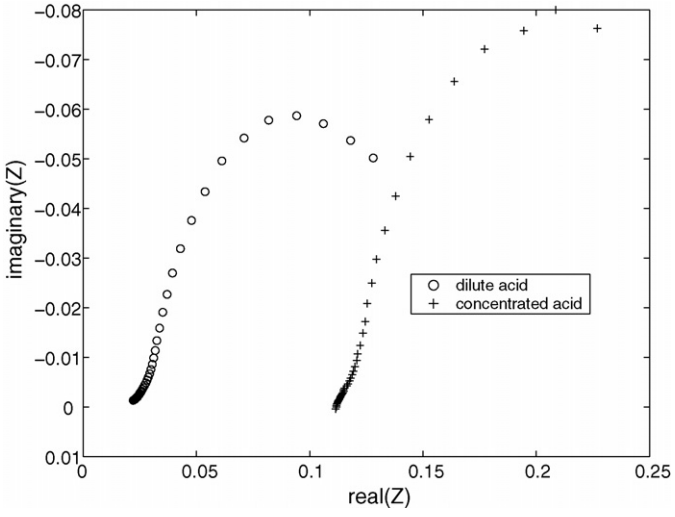

Fig. 24. Experimental Nyquist plot of concentrated acid cathode at higher overpotential $\eta = -0.2$ V.

6.1. Effect of active area

Experimental output as depicted in Fig. 14 showing 1% Pt loaded carbon performance against standard 10% Pt as discussed previously shows peak phase angle of 1% Pt has shifted towards right hand side of that of the standard 10% Pt. Interestingly the simulated effect of a similar case as depicted in Fig. 5 also shows very similar trend. The discussion done in the previous section referring to Fig. 5 thus matches well with the experimental findings. The possible reasons for the simulated results are already discussed in Section 4.

6.2. Analysis of fouling phenomena

Experimental Nyquist plot of the fouled electrode as discussed before and shown in Figs. 17 and 19 at overpotentials of 100 and 200 mV, respectively showed the same electrolytic conductivity. This is observed from the high frequency side impedance, i.e., the left most impedance, of the fouled electrode. This matches with that of the standard electrode for both overpotentials. This suggests that the electrolyte for both the cases (fouled and standard one) are similar and the leaching of the organic materials from the fouled electrode has not changed the electrolyte.

Through the model and the experimental results, possible mechanisms of the fouling phenomena are studied. Two hypotheses for fouling are considered:

- The fouling of the electrode could be due to over wetting of the bigger pores which otherwise are kept dry by Teflon and act as gas feeder pores. This leads to effectively bigger agglomerates by flooding of interspace between the small agglomerates.
- Partial blocking of the sites by the carbon char/polymeric gel inside the fine pores.

To check the two hypotheses, initially, the experimental and simulated results at 100 mV overpotential are studied. A case similar to the second hypothesis, is depicted in the simulated phase angle plot in Fig. 6, as discussed in Section 4. In this scenario it is considered that although some sites are not available for reaction, they are not out of electrochemical path and hence offer same double layer capacitance. It can be seen, that the experimental peak phase angle of the fouled electrode as depicted in Fig. 18 for an overpotential of 100 mV has shifted to the left hand side. The effect is quite similar to that observed in the simulated Fig. 6 as described before. The other mechanism for fouling based on the first hypothesis; that is wetting of dry pores by the alcohol leading to an overall increase of the agglomerate size is also analyzed. If the agglomerate size is bigger, then much of the active sites will be deeply embedded and will not receive enough reactant resulting in loss of performance of the electrode. Simulated effect of pore size change depicted in Fig. 4 at an overpotential of 100 mV as described before also shows that as the agglomerate size increases, the peak phase angle shifts to the left, matching with the fouled electrode trend at 100 mV as depicted in Fig. 18.

Thus both the fouling mechanisms, viz., area blocking with unchanged capacitance and agglomerate fusion, analyzed using the model match with experimental data. If both the effects are analyzed closely, they are bound to create less active area with almost unchanged double layer capacitance. For agglomerates fusing to yield larger agglomerates, the deep seated active sites will receive very less reactant, but will offer double layer capacitance. The model thus quite rightly shows similar effect towards fouling. In an attempt to separate the two effects, experimental and simulated results at higher overpotential (200 mV), are taken into consideration. At such high overpotential, the double layer capacitance changes/distorts quite a bit [17]. Fig. 20 depicts the experimental phase angle plot of the electrode at 200 mV. The phase angle plot shows peak phase angle for the fouled electrode shifting to the left hand side. Thus the trend remains same like the lower overpotential experimental result depicted in Fig. 18.

Fig. 26 depicts the simulated case for the second hypothesis where the active sites are reduced but with same double layer capacitance. The simulation result shows lower active area peak phase angle at the right hand side of that of the higher area one. Thus although at lower overpotential the trend of phase angle matched with the experimental one, at higher overpotential it is reversed when compared to the experimental result as shown in Fig. 20. Fig. 27 depicts the simulated phase angle response for agglomerate fusion which is similar to the first

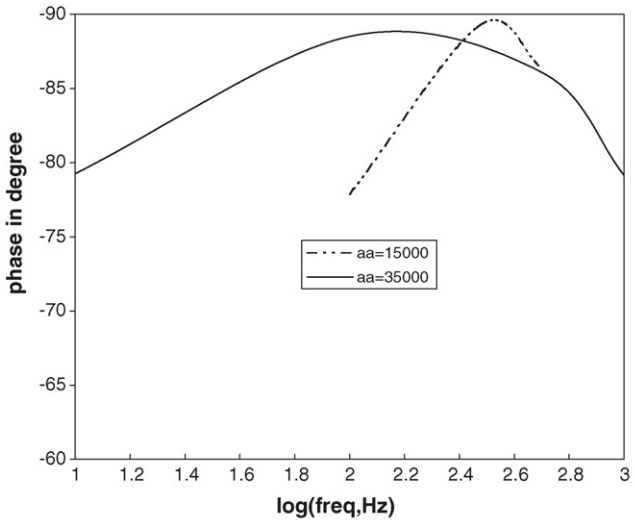

ε	R_{agg}	a_a	κ_{el}	κ_{agg}	η
20e-06	5e-04	35000	1e-06	0.4	-0.2
20e-06.(35000/15000)	5e-04	15000	1e-06	0.4	-0.2

Fig. 26. Simulated phase angle plot for different active areas but same total double layer capacitance at a higher overpotential.

hypothesis which considers agglomerate fusion at an overpotential of 200 mV. It can be seen that the bigger agglomerate peak phase angle is shifted to the left hand side of that of the smaller agglomerate. This trend is similar to the experimental finding as shown in Fig. 20. Thus, for this case, it might be concluded that the electrode fails primarily due to wetting of dry pores by furfuryl alcohol. However at high overpotential values, the double layer capacitance increases and hence for more certain resolution, detailed functionality of the double

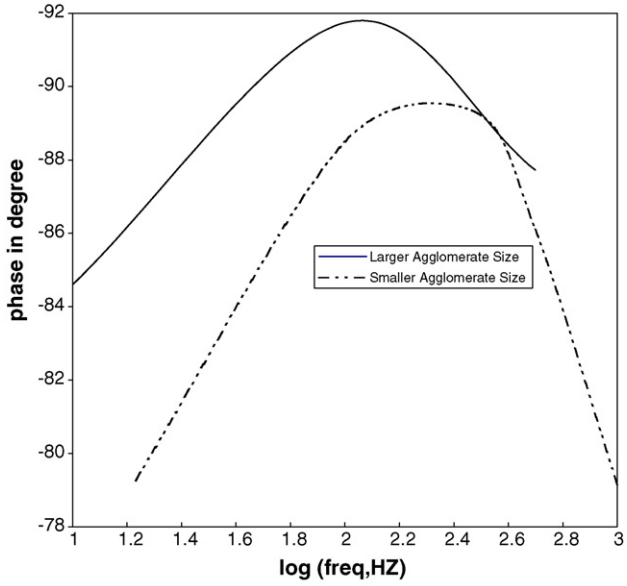

ε	R_{agg}	a_a	κ_{el}	κ_{agg}	η
20e-06	5e-03& 5e-04	35000	1e-06	0.4	-0.2

Fig. 27. Simulated phase angle plot for different agglomerate sizes at higher overpotential.

layer capacitance with respect to overpotential may have to be considered.

6.3. Electrolyte conductivity

Another important parameter is the phosphoric acid conductivity. The experimental phase angle plot at 100 mV overpotential is depicted in Fig. 23 as described before. It can be seen that the dilute acid which is of higher conductivity has the peak phase angle to the right hand side of the concentrated acid peak phase angle. Fig. 10 depicts the simulated phase angle plot, which shows the phase angle response of two different electrolyte conductivities at 100 mV as discussed in Section 4. The higher conductivity simulation shows peak phase angle to the right side of that of the low conductivity one. This effect is similar to the experimental result. Fig. 25 depicts experimental response of dilute and concentrated acids at a higher overpotential (200 mV). Simulated results as depicted in Fig. 9 at 200 mV overpotential also supports similar trend. Thus the model successfully matches the peak phase angle trend for the case of general change of acid resistance/concentration.

7. Conclusions

In this work, information related to peak phase angle position is used to analyze failure mechanisms in PAFC cathode. The position of the peak phase angle at various overpotentials are determined at different experimental conditions and the findings are explained with a simple mathematical model. This exercise shows that instead of trying to match the entire impedance/admittance of the electrode through transmission line like model – which is difficult to analyze – a simple agglomerate mathematical model can be quite useful for cathode diagnostics. The use of peak phase angle position as an analysis tool allows the comparison of different sized electrodes. Analysis of the simple agglomerate model allows direct understanding of the system. However, certain limitations of the simple model should be understood before analysis. The model will not determine many of the inter-agglomerate changes. For example, as a new electrode ages, more agglomerate per unit catalyst layer volume gets wetted. This effect cannot be characterized using the agglomerate model. However, if the wettability of the agglomerates increases, i.e., partially flooded agglomerates get fully flooded (which happens as a new electrode ages), this effect can be analyzed using this simple model.

Table 2
Brief summary of the effects studied

Parameter	Overpotential	Peak shift
Surface area	At low overpotential	As a_a increases, peak shifts left
Agglomerate size	At low to medium overpotential	As size increases, peak shifts left
Acid conductivity	At low to medium overpotential	As conductivity increases, peak shifts right
Capacitance per unit area	At low overpotential	No appreciable change in peak position
Capacitance adjusted	At low overpotential	As a_a increases, peak shifts right
Surface area	At medium overpotential	As a_a increases, peak shifts left

It can be seen that for many cases the actual peak phase angle of the experimental electrode and the simulated one appear at different parts of the frequency spectrum. This is primarily due to two reasons. The PAFC cathode holds acid even in some dry zones particularly near the electrolyte side. This electrolyte holdup changes with electrode aging and accordingly the performance of the cathode changes. Oxygen availability is negligible due to very high liquid diffusion resistance in most of these portions. Thus, mostly capacitive current is generated from these zones. Further, the electrode has various sized agglomerates and due to diffusion resistance the oxygen partial pressure might be low in some of the agglomerate regions. Thus the total capacitance to the resistance ratio of the entire electrode differs from single electrolyte coated agglomerate. This added capacitance is mostly responsible for the peak phase angle position to be shifted generally to a lower frequency when compared to the simulations.

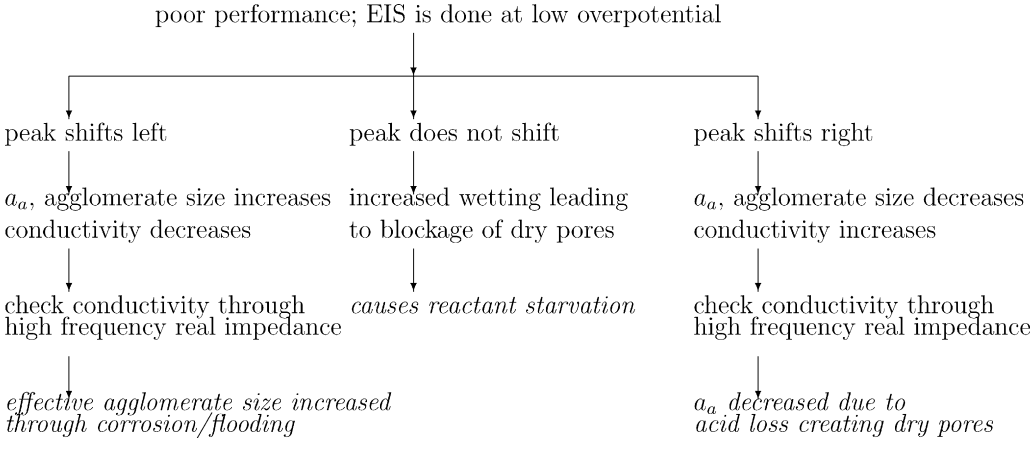

Fig. 28. A simplified decision tree.

In order to perform a more comprehensive analysis, the entire model as proposed in our previous work [2] needs to be analyzed. This may require heavy computation, but once tuned, will yield more fundamental insights, particularly for bigger cathodes. For bigger cathodes, reactant depletion will have a significant effect and EIS data in tandem with the comprehensive model might be able to identify such situations. For simple failure analysis, the simple agglomerate model with the proposed diagnostic marker shows encouraging results. The implementation methodology should be to analyze the phase angle response at various overpotentials of the standard and the faulty electrodes. A decision tree can then be designed based on this analysis. This tree can also be used to understand operation problems online. Table 2 summarizes the work presented here. Based on the summarized results, Fig. 28 shows a simplified decision tree. However it should be understood that many of the effects may occur simultaneously and to isolate them one needs to perform much more detailed analysis with a comprehensive model.

References

[1] W. Vielstich, A. Lamm, H.A. Gasteiger (Eds.), Handbook of Fuel Cells, Fundamentals, Technology and Applications, vol. 4, John Wiley and Sons Ltd., 2003, ISBN 0-471-49926-9.
[2] S.R. Choudhury, S.R. Choudhury, J. Rangarajan, R. Rengaswamy, Step response analysis of phosphoric acid fuel cell (PAFC) cathode through a transient model, J. Power Sources 140 (2005).
[3] L.G. Austin, M. Ariet, R.D. Walker, G.B. Wood, R.H. Comyn, Ind. Eng. Chem. Fund. 4 (1965).
[4] H. Celikar, M.A. Al-saleh, S. Gultekin, A.S. Al-zakri, A mathematical model for performance of raney nickel metal gas diffusion electrodes, J. Electrochem. Soc. 138 (6) (1991).
[5] F.G. Will, J. Electrochem. Soc. 110 (1963).
[6] E.A. Grens, Ind. Eng. Chem. 5 (1966).
[7] J. Giner, C. Hunter, J. Electrochem. Soc. 116 (1969).
[8] R.P. Iczkowski, M.B. Cutlip, J. Electrochem. Soc. 127 (1980).
[9] K. Yamashita, T. Taniguchi, Agglomerate model for dc and ac response of phosphoric acid fuel cell cathode, J. Electrochem. Soc. 145 (1) (1998).
[10] M.L. Perry, J. Newman, E.J. Cairns, Mass transport in gas diffusion electrodes: a diagnostic tool for fuel cell cathodes, J. Electrochem. Soc. 145 (1) (1998).
[11] W. Jenseit, O. Bohme, F.U. Leidich, H. Wendt, Impedance spectroscopy: a method for in situ characterization of experimental fuel cells, Electrochim. Acta 38 (14) (1993).
[12] A.J. Bird, L.R. Faulkner, Electrochemical Methods Fundamentals and Applications, 2nd ed., John Wiley and Sons, 2001.
[13] S.R. Choudhury, M.B. Deshmukh, R. Rengaswamy, A two dimensional steady-state model for phosphoric acid fuel cells (PAFC), J. Power Sources 112 (2002).
[14] G.W. Castellan, Physical Chemistry, Narosa Publishing House, 1983.
[15] Pt/rh/fe alloy catalyst for fuel cells and a process for producing the same, US Patent No. 6,165,635, 2000.
[16] D. Chin, H.H. Chang, On the conductivity of phosphoric acid electrolyte, J. Appl. Electrochem. 19 (1989) 95–99.
[17] A.S. Arico, V. Alderucci, V. Antonucci, S. Ferrara, V. Recupero, N. Giordano, K. Kinoshita, ac impedance spectroscopy of porous gas diffusion electrode in sulphuric acid, Electrochim. Acta 37 (3) (1992).